Real-Time Detection and Classification of Power Quality Problems Based on Wavelet Transform

F. R. Zaro[1*], M. A. Abido[2]

[1] Electrical Engineering Department, Palestine Polytechnic University, Hebron, Palestine
E-mail: fzaro@ppu.edu
[2] Electrical Engineering Department, King Fahd University of Petroleum and Minerals, Dhahran, Saudi Arabia

Abstract— A new technique for real-time power quality (PQ) disturbances detection and classification based on wavelet multi-resolution analysis (MRA) is presented in this paper. The detection of start time, end time and duration of PQ event is based on the finest detail level of MRA while the classification of the event is based on the coarsest approximation level of MRA. LabVIEW platform has been used to implement the proposed technique in a laboratory setup. Several voltage events: interruption, swell and sag have been generated to test the performance of the proposed technique. The experimental results demonstrate the superiority, accuracy, and robustness of the proposed method in detecting the details of the voltage events as well as the event type classification. The effectiveness, accuracy and robustness of the proposed technique in the detection and classification of the PQ events have been demonstrated by experimental results. Moreover, the proposed technique shows a significant reduction in execution time with less complexity compared to conventional methods, for that the proposed technique is more suitable for online detection and classification applications.

Keywords— Multi-resolution wavelet analysis; Power quality; Voltage events.

1.   INTRODUCTION

Modern distributed renewable power sources contain a large number of power electronic devices. The increasing use of such devices contributes to the arising power quality (PQ) problems that have a negative impact on the power system reliability [1]. Therefore, developing an efficient monitoring system for PQ problems will help better understand and identify the cause of PQ disturbances. The international organizations working on PQ issues such as IEEE and IEC recommend guidelines for PQ monitoring [2, 3].

Along with technology advances, many companies worldwide applied minimization/elimination measures for PQ problems to increase their productivity. Information technology services and the continuous process industry are the most affected areas by PQ problems; voltage event huge financial losses may happen, with the consequent loss of productivity [4].

The automated classification of PQ disturbances is a significant issue for real-time PQ monitoring especially in the deregulated era. The continuous wavelet transform (CWT) and Fourier transform (FT) have been proposed to detect and analyze PQ disturbances [5, 6]. However, CWT and FT have some limitations for on-line PQ monitoring applications. CWT is a redundant transformation where the excessive amount of information may affect the identification and classification process. On the other hand, since FT has a fixed frequency resolution, it is not suitable for the

* Corresponding author

characterization of voltage transient phenomena that needs a flexible frequency resolution [7]. Artificial intelligence and machine learning is presented for the classification of PQ disturbances as powerful tools [8-12].

The discrete wavelet transforms (DWT) is an effective tool for detection, localization, and classification of PQ disturbances [13-15]. The squared WT coefficients at each level are utilized to create a unique feature whereas the dyadic-orthonormal WT was used to detect and localize different PQ disturbances [16].

Such a feature is used to classify different PQ disturbances using a proper classification tool. The wavelet multiresolution signal decomposition was proposed for analyzing PQ transient events. Generally speaking, some features have been proposed in literature to classify different PQ problems. These include: (a) the standard deviation curve at different resolution levels [17]; (b) the delta standard deviation multiresolution analysis at each decomposition level [18]; (c) the energy distribution of the wavelet part at each decomposition level [19], [20]; (d) the inductive inference approach [21]; and (e) the obtained wavelet coefficients at each decomposition level [22]. It is worth mentioning that the reported approaches utilize all the wavelet decomposition levels to extract the feature that can be used to classify PQ disturbances. Because the proposed approach in this study utilizes less information, it is considered more suitable for online applications.

This paper presents a new wavelet multiresolution analysis-based real time detection and classification technique for voltage events developed on LabVIEW platform. In the proposed technique, the detection of start time, end time, and duration of PQ event is based on the finest detail level of MRA while the classification of the event is based on the coarsest approximation level of MRA. The proposed technique is applied on several typical short duration voltage events: interruption, sag, and swell. The performance of the proposed technique is also tested under the presence of harmonic contents and high frequency noise. This paper is organized as follow: Wavelet application to power quality is discussed in Section 2. Section 3 presents the proposed method. The experimental setup to assess the proposed method is described in Section 4. Section 5 provides validation of the proposed method. The experimental results are presented and discussed in Section 6.

2. WAVELET APPLICATION TO POWER QUALITY

Multi-resolution analysis (MRA) is an effective approach for analyzing the signal mostly where it is necessary to check different frequency components separately. However, MRA is able to reveal aspects of data such as breakdown points, discontinuities, trends, and self-similarity whereas other tools for signals analysis would be missed [23, 24]. Also, MRA is an efficient tool to extract features from PQ disturbance data [7, 25].

2.1. Detection and Localization

MRA can be used to compose the distorted signal into different resolution levels. At the finer resolution levels, any changes in the smoothness of the signal can be

detected and localized. Generally, the detection and localization of the PQ disturbance can be achieved at the first finer decomposition levels. However, the classification process based on feature extraction can be accomplished at the coarser resolution levels [26].

2.2. Classification

According to the patterns of energy distribution across multiple frequency bands, different PQ disturbances can be classified perfectly.

If the used wavelet and scaling functions form an orthonormal set of basis, then the Parseval's theorem relates the energy of the distorted signal to the values of the coefficients [27]. Thus the energy of the signal can be partitioned as:

$$\int |f(t)|^2 \, dt \; = \; \sum_k \left| A_{j0}(k) \right|^2 + \sum_{j \le j_0} \sum_k \left| D_j(k) \right|^2 \tag{1}$$

where A_{j0} and D_j represent the coarsest approximation level with the fundamental frequency and the detail level of the jth decomposition level respectively; and k represents the wavelet coefficients at each decomposition level.

2.3. Characterization of Short-Duration Voltage Events

For updating values, the rms methods depend on the window length and time interval that make the magnitude and duration of a voltage event inaccurate [28-30]. The MRA is presented to produce more accurate results that would be useful for determining the causes of such events [31]. In this work, the proposed method utilizes MRA with less information and thus; it is more suitable for on-line implementation.

3. THE PROPOSED METHOD

In general, approximation and details components can be utilized to reformulate a signal f as follows:

$$f = \sum_k a_{j_0 k} \varphi_{j_0 k} + \sum_{j \le j_0} \sum_k d_{jk} \psi_{jk} \, , \tag{2}$$

where

$$\psi_{jk}(t) = 2^{-j/2} \psi \left(2^{-j} t - k \right) \tag{3}$$

$$\varphi_{j_0 k}(t) = 2^{-j_0/2} \varphi \left(2^{-j_0} t - k \right) \tag{4}$$

$\psi(t)$ represents the mother wavelet; and $\varphi(t)$ represents the scaling function.

$$d_{jk} = \int f(t) \psi_{jk}(t) dt \tag{5}$$

$$a_{j_0 k} = \int f(t) \varphi_{j_0 k}(t) dt \tag{6}$$

It is observed that coefficients corresponding to orthogonal signals are orthogonal sequences. Suppose $f, \tilde{f}$ are orthogonal signals. i.e.

$$\langle f, \tilde{f} \rangle = 0 \, , \quad \left(\int f(t) \tilde{f}(t) \, dt = 0 \right) \tag{7}$$

where

$$f = \sum_{j,k} d_{jk}\psi_{jk} \quad , \qquad \tilde{f} = \sum_{j',k'} \tilde{d}_{j'k'}\psi_{jk'} \tag{8}$$

this yield:

$$0 = \langle f, \tilde{f} \rangle = \langle \sum_{j,k} d_{jk}\psi_{jk} \ , \sum_{j',k'} \tilde{d}_{j'k'}\psi_{jk'} \rangle = \sum_{j,k} \sum_{j',k'} d_{jk}\tilde{d}_{j'k'} \langle \psi_{jk}, \psi_{jk'} \rangle \tag{9}$$

since

$$\langle \psi_{jk}, \psi_{jk'} \rangle = \delta_{jkj'k'} \tag{10}$$

therefore;

$$0 = \sum_{jk} d_{jk}\tilde{d}_{j'k'} \tag{11}$$

according to Eq. (11); (d_{jk}) and $(\tilde{d}_{j'k'})$ are orthogonal sequences.

The inner product of a sinusoidal signal (f) with a distorted signal that has a high frequency disturbance (g+h) eliminates the effect of the high frequency disturbance (h) as follows:

$$\langle f, g + h \rangle = \langle f, g \rangle + \langle f, h \rangle = \langle f, g \rangle \tag{12}$$

The voltage events such as: sag, swell, and interruption are scaled versions of the original pure signal over the disturbance interval (I_d). Therefore, voltage events should correlate well over I_d with the pure sinusoidal signal at the coarsest approximation level. The following symbols have been adopted:

- f: pure signal.
- $(d_{jk})_{k \in \mathbb{Z}}$: wavelet detail coefficients of the pure signal at the scale level j.
- s: disturbance signal, which is zero outside I_d, that is $s(t) = 0 \ for \ t \notin I_d$. I_d, will be called the support of s.
- $(\tilde{d}_{jk})_{k \in \Delta_j}$: wavelet coefficients of the disturbance signal at the coarsest approximation level j_0 over the disturbance interval I_d, where

$$\Delta_j = \{k: \text{supp } \psi_{jk} \subseteq I_d\} \tag{13}$$

To discriminate between the three types of disturbances, the following procedure is proposed:

1. compute:

$$\left\| (d_{j_0k}) \right\|_{\Delta_{j_0}} = \left(\sum_{k \in \Delta_{j_0}} d_{j_0k}^2 \right)^{\frac{1}{2}} \tag{14}$$

$$\left\| (\tilde{d}_{j_0k}) \right\|_{\Delta_{j_0}} = \left(\sum_{k \in \Delta_{j_0}} \tilde{d}_{j_0k}^2 \right)^{\frac{1}{2}} \tag{15}$$

$$r = \frac{\left\| (\tilde{d}_{j_0k}) \right\|_{\Delta_{j_0}}}{\left\| (d_{j_0k}) \right\|_{\Delta_{j_0}}} \tag{16}$$

2. if $(1 - \varepsilon) \leq r \leq (1 + \varepsilon)$ then there is no event, (ε is a preassigned threshold; assumed in this work $\varepsilon = 0.1$).
3. if $r > (1 + \varepsilon)$ the disturbance corresponds to a swell.
4. if $\varepsilon \leq r < (1 - \varepsilon)$ the disturbance corresponds to a sag.
5. if $r < \varepsilon$, then

a. compute F_j as:

$$F_j = \sum_{k \in \Delta_j} d_{jk} \tilde{d}_{jk} , \qquad j = 1, \dots, j_0 - 1 \tag{17}$$

b. check the following condition:

$$\sum_{j=1}^{J} F_j^2 \le \varepsilon^2 \tag{18}$$

If satisfied then the disturbance corresponds to an interruption. Otherwise, it corresponds to some other high frequency disturbances. Fig. 1 shows the flow chart of the proposed approach.
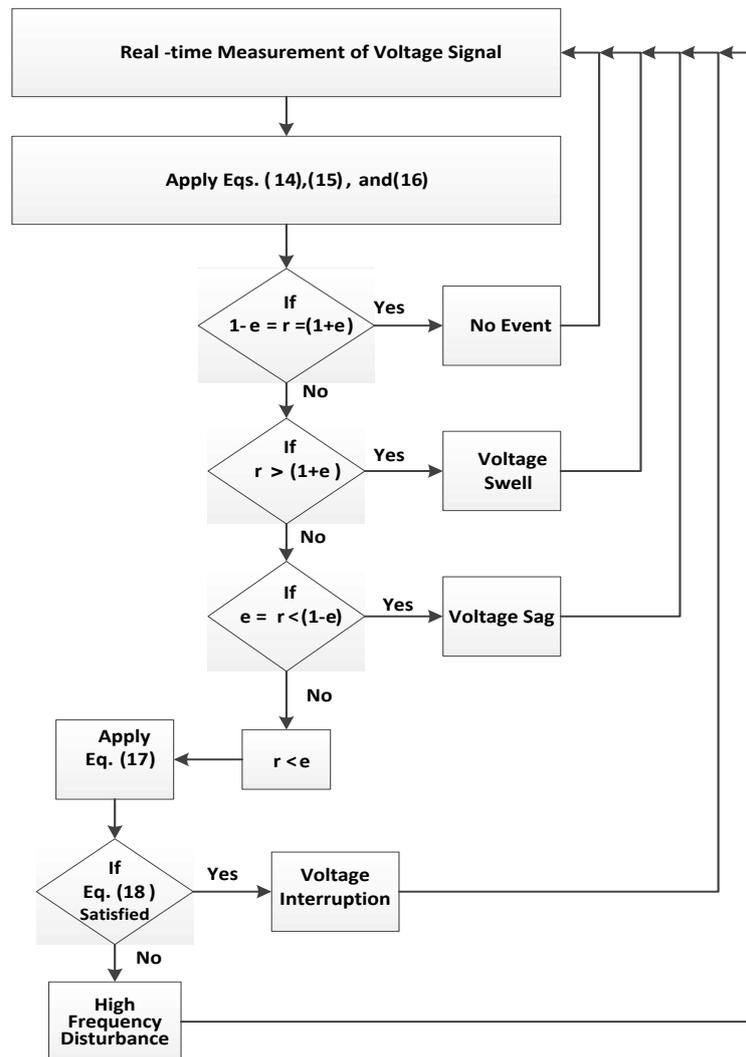
Fig. 1. Flow chart of the proposed method.

The mother wavelet Daubechies 6 (db6) is the most appropriate mother wavelet used to detect voltage events [32-34]. For that reason, db6 has been employed in the proposed approach to detect and classify all the transient disturbances in the distorted signal.

The various PQ disturbances are generated according to the parametric equations given in Table 1. The step input function u(t) is used to vary the disturbance duration.

The PQ disturbances are generated by varying the amplitude of disturbances as well as duration of the event.

Table 1. Modeling of PQ disturbances and their parameter variations [13].

Disturbance	Modeling	Parameter
Sag	$x(t) = A(1 - \alpha(u(t-t_1) - u(t-t_2))) \sin(\omega t)$	$0.1 < \alpha < 0.9$, $T < t_2 - t_1 < 11T$
Swell	$x(t) = A(1 + \alpha(u(t-t_1) - u(t-t_2))) \sin(\omega t)$	$0.1 < \alpha < 0.9$, $T < t_2 - t_1 < 11T$
Harmonics	$x(t) = A(\alpha_1 \sin(\omega t)) + \alpha_3 \sin(3\omega t)$ $+ \alpha_5 \sin(5\omega t) + \alpha_7 \sin(7\omega t)$	$0.05 < \alpha_1, \alpha_3, \alpha_5 < 0.15$, $\sum \alpha_i^2 = 1$
Interruption	$x(t) = A(1 - \alpha(u(t-t_1) - u(t-t_2))) \sin(\omega t)$	$0.9 < \alpha < 1$, $T < t_2 - t_1 < 11T$
Sag and harmonics	$x(t) = A(1 - \alpha(u(t-t_1) - u(t-t_2)))\alpha_1 \sin(\omega t)$ $\alpha_3 \sin(3\omega t) + \alpha_5 \sin(5\omega t) + \alpha_7 \sin(7\omega t)$	$0.1 < \alpha < 0.9$, $T < t_2 - t_1 < 11T$ $0.05 < \alpha_1, \alpha_3, \alpha_5 < 0.15$, $\sum \alpha_i^2 = 1$
Swell and harmonics	$x(t) = A(1 + \alpha(u(t-t_1) - u(t-t_2)))\alpha_1 \sin(\omega t)$ $\alpha_3 \sin(3\omega t) + \alpha_5 \sin(5\omega t) + \alpha_7 \sin(7\omega t)$	$0.1 < \alpha < 0.9$, $T < t_2 - t_1 < 11T$ $0.05 < \alpha_1, \alpha_3, \alpha_5 < 0.15$, $\sum \alpha_i^2 = 1$

4. THE EXPERIMENTAL SETUP

Fig. 2 shows the experimental setup that consists of a programmable AC source, NI Compact-RIO, panels housing current transformers with load connectors, programmable electronic loads, and workstation running LabVIEW.

Fig. 2. The experimental setup in a power quality laboratory.

4.1. Voltage Input Module

The NI-9225 module has been selected to measure rms voltage directly from the line. It is an analog input module consisting of 3 channels; it can directly measure rms phase voltage up to 300V. Fig. 3 shows the NI-9225 voltage analog input module. It is directly connected to the main power feeders to measure the instantaneous phase voltages for the three phases as shown in Fig. 4.
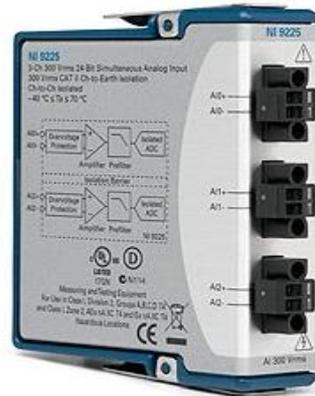
Fig. 3. The NI-9225 voltage analog input module.
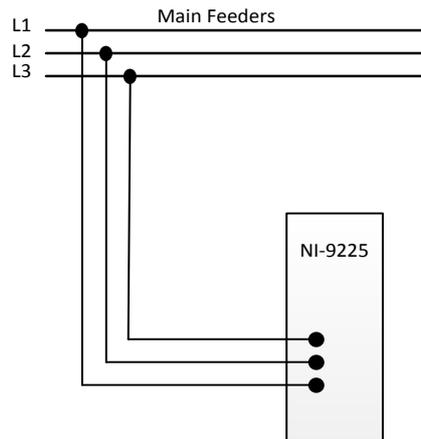
Fig. 4. The general connection diagram of the NI-9225 voltage analog input module with power feeders.

4.2. Current Input Module

The NI-9227 module has been selected to measure the current. It has 4 channels; and can measure rms current directly up to 5 A. On the other hand, most of the rms current values in the system are larger than 5A. For this reason, current transformer (CT 200/5 A) has been used to measure currents through the module in each phase as well as in the neutral line. Fig. 5 shows the NI-9227 current analog input module. It is connected to the main power feeders and the neutral line through 4 CTs to measure the instantaneous current for each line as well as for the neutral line as shown in Fig. 6.
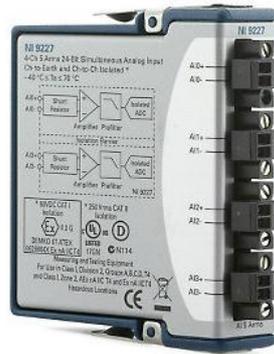
Fig. 5. The NI-9227 current analog input module.
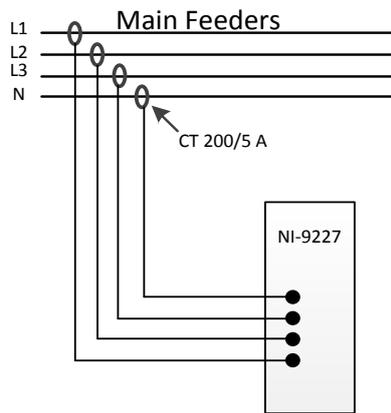
Fig. 6. General connection diagram of the NI-9227 current analog input module with power feeders.

4.3. Sourcing Digital Output Module

The NI-9476, shown in Fig. 7, is a 32-channel, 500 μs sourcing digital output module. It has been selected to perform software-timed and static operations in the controlling system. It is directly connected to the relays of the switching control panel of the devices and loads. Each channel can drive up to 250 mA continuous current on all channels simultaneously with 24V signals. However, each relay in the switching control panel is fed by two channels to make sure that the continuous output current of each channel will not exceed the limits (250mA). Fig. 8 shows the connection philosophy of the digital output module with the relays in the developed system.

Fig. 7. The NI-9476 digital output module.
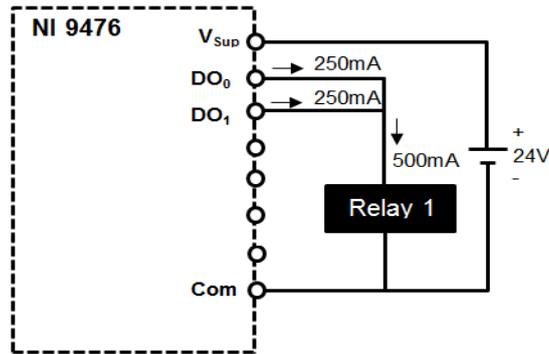
Fig. 8. The connection diagram of the NI-9476 digital output module with a control relay.

4.4. Analog Output Module

The NI-9264 is a 16-channel analog output module with -10V to +10V voltage range. It has been selected to control the mitigation device operation. The actual voltage signal of the controller of the mitigation device is provided by a channel of NI-9264. Figs. 9 and 10 show the selected analog output module and connection diagram of the module with a controller, respectively.

Fig. 9. The NI-9264 analog output module.
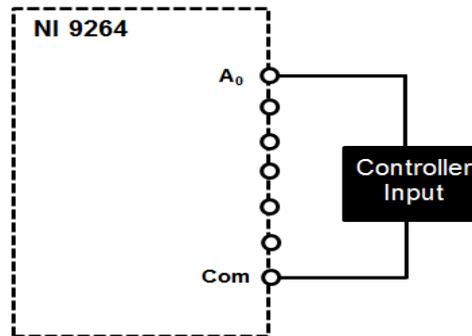
Fig. 10. Connection diagram of the controller to the NI-9264 analog output module.

4.5. Real-time Controller

The intelligent real-time embedded controller NI cRIO-9024 is shown in Fig. 11. It is a 800 MHz processor, 4 GB nonvolatile storage, 512 MB DDR2 memory. The controller runs LabVIEW Real-time for deterministic control, data logging, and analysis.

The controller has been installed on the cRIO chassis. The static IP address has been assigned to communicate the host computer with the controller over a standard Ethernet connection for remote monitoring and accessing. The MAX software is used for configuring IP settings for the controller and installing LabVIEW Real-Time software and device drivers on the controller. The system clock of the cRIO-9024 is synchronized with the internal high-precision real-time clock to provide timestamp data to the controller.

Fig. 11. The NI cRIO-9024 real-time controller.

4.6. Reconfigurable FPGA Chassis

The selected model of reconfigurable FPGA chassis in this application is NI cRIO-9118 that is shown in Fig. 12. The selected chassis is 8-slot and it accepts any cRIO I/O module. It has an ability to automatically synthesize custom control and signal processing circuitry using LabVIEW. It is directly connected to the I/O module for high-performance access to the I/O circuitry of each module. A local PCI bus connection provides a high-performance interface between the RIO FPGA and the real-time processor.

Fig. 12. Reconfigurable FPGA Chassis_ NI cRIO-9118.

System functionality can be changed and upgraded by changing the LabVIEW FPGA module code and rebuilding and compiling a new bit stream configuration to the FPGA hardware. Fig. 13 shows the ultimate virtual instrument (VI) block diagram of the proposed voltage monitoring system.
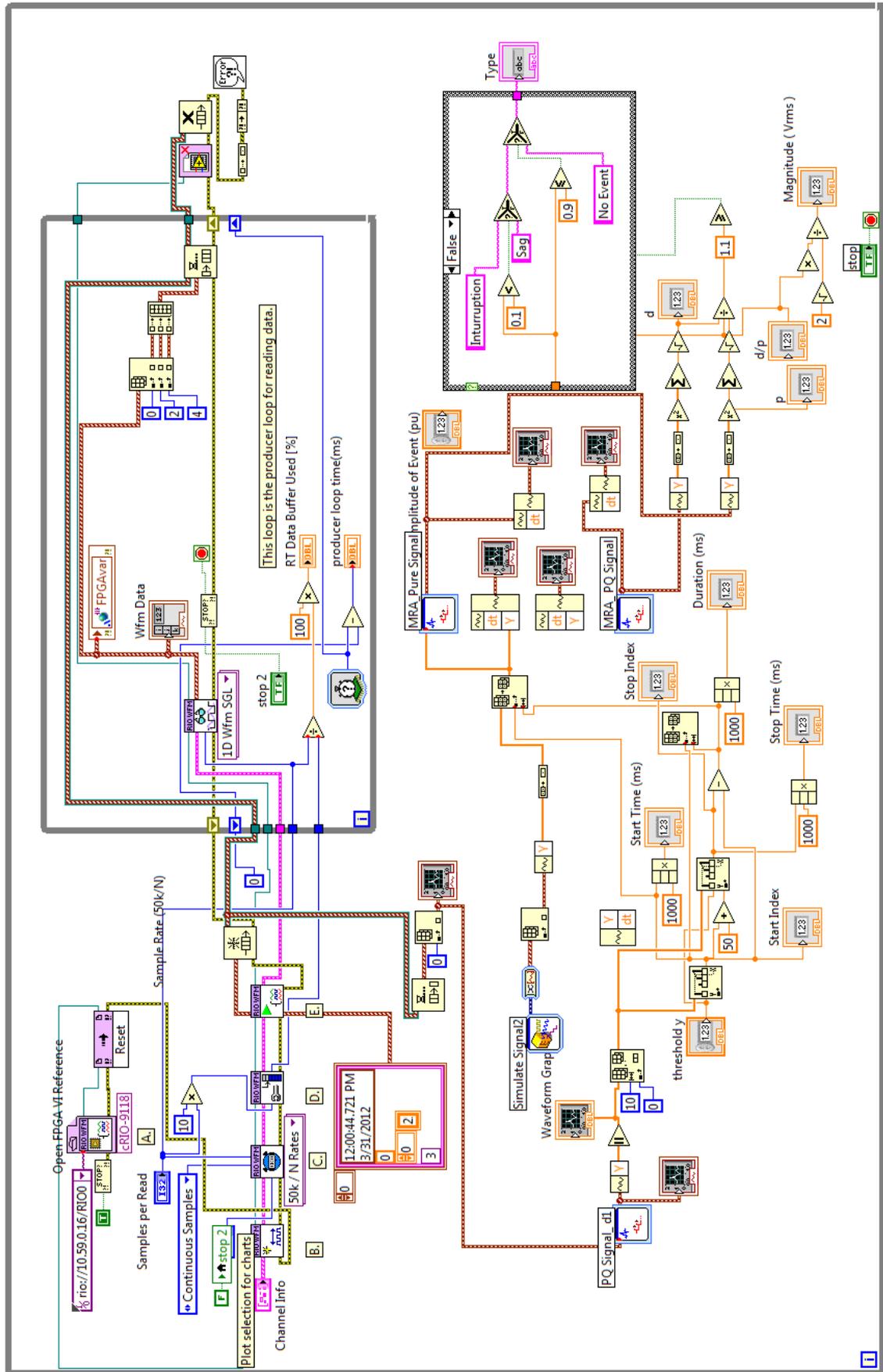
Fig. 13. Virtual instrument of the proposed method for the voltage monitoring system.

5.   VALIDATION OF THE PROPOSED METHOD

The conventional calculation method of rms voltage based on DWT in a power system can be calculated as follow:

$$V_{rms} = \sqrt{V_{j_0}{}^2 + \sum_{j \leq j_0} V_j{}^2} \qquad (19)$$

where V_{j0} represents the rms voltage value of the coarsest approximation wavelet decomposition level j_0 which includes the fundamental frequency; V_j represents the rms voltage value of each detail wavelet decomposition level j higher than or equal to j_0. The conventional method of calculating rms value based on DWT uses all of the detail levels as well as the coarsest levels as given in Eq. (19). However, the proposed approach calculates the rms value using the coarsest approximation level solely.

Fig. 14 displays the first six decomposition levels of a signal. According to Eq. (19), V_{j0} represents the rms voltage of the sixth approximation level (A_6); and $\{V_j\}$ represents $\{V_{D1}, V_{D2} \ldots V_{D6}\}$. Therefore Eq. (19) can be rewritten as:

$$V_{rms} = \sqrt{V_{A6}{}^2 + \sum_{j=1}^{6} V_{Dj}{}^2} \qquad (20)$$
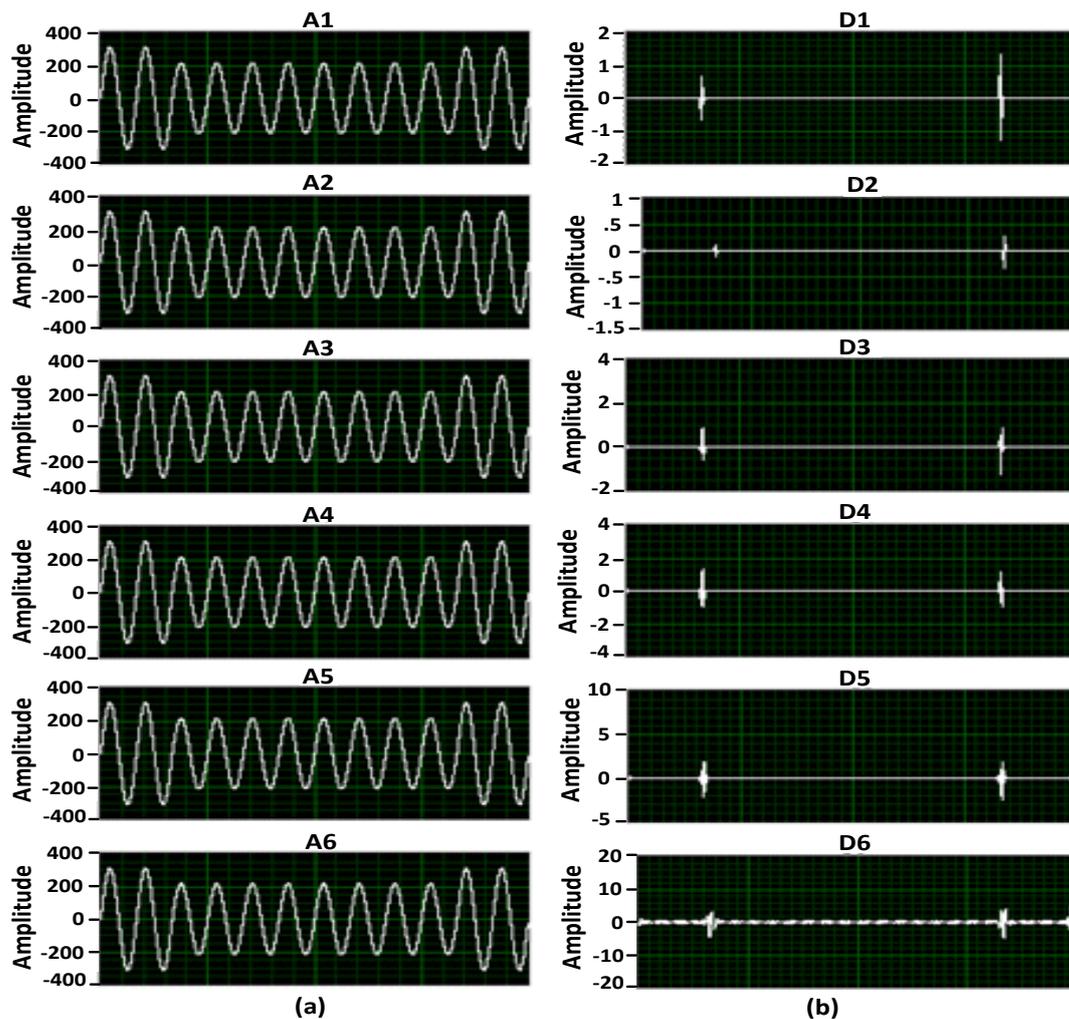
Fig. 14. The first six decomposition levels of the test signal: a) approximation levels; b) detail levels.

6.   EXPERIMENTAL RESULTS

The programmable AC source has been utilized to generate the test signal that is used to evaluate the performance of the proposed approach in real-time. The test voltage signal 220 V/60Hz 12 cycles with 166 sample/cycle has been generated to calculate the rms voltage value. Applying the conventional DWT method, at 33.2 ms voltage event is started and continued until 166 ms (event duration 8 complete cycles). The voltage events which have been checked include: interruption, sag, and swell. Each one of them is carried out for three times; and the average results are adopted in this study.

6.1.   Case 1- Voltage Interruption

The voltage interruption event with a value of 11 V_{rms} is started at 33.2 ms and ended at 166 ms. The voltage event details that have been detected, characterized, and classified by the proposed method are shown in Fig. 15(a). The accuracy of the proposed approach in estimating the details of the voltage event reaches to more than 99.6%. The proposed method is utilized to classify the voltage event type. Fig. 15(b) shows the output of a monitoring system that measured the waveform corresponding to the voltage interruption response. The first detail wavelet decomposition level (D_1) shown in Fig. 15(c) contains two peaks that have been utilized to detect voltage event details. Fig. 15(d) and Fig. 15(e) show the waveforms of the distorted and pure voltage signals within the event duration, respectively. Fig. 15(f) shows the coarsest approximation level (A_6) of the distorted voltage signal during the voltage event duration. Fig. 15(g) shows the coarsest approximation level (A_6) of the pure voltage signals within the voltage event duration.

6.2.   Case 2- Voltage Sag

The voltage sag with a value of 110V_{rms} is started at 33.2 ms and ended at 166 ms. The estimated details of the voltage sag event using the proposed approach are shown in Fig. 16(a) which shows high accuracy in the estimation of the voltage sag event details, reaching to more than 99.7%. The monitoring system corresponding to the voltage sag event is shown in Fig. 16(b). The characterization and classification of the voltage sag according to the analyzed waveforms are shown in Fig. 16(c) to Fig. 16(g).

6.3.   Case 3- Voltage Swell.

The voltage swell with a value equal to 286 V_{rms} is started at 33.2 ms and ended at 166 ms. Fig. 17(a) shows the results obtained using the proposed approach in estimating the details of the voltage swell event with an accuracy of more than 99.6%. The monitoring system behavior in response to the voltage swell event is shown in Fig. 17(b). The characterization and classification of the voltage swell according to the analyzed waveforms are shown in Fig. 17(c) to Fig. 17(g).
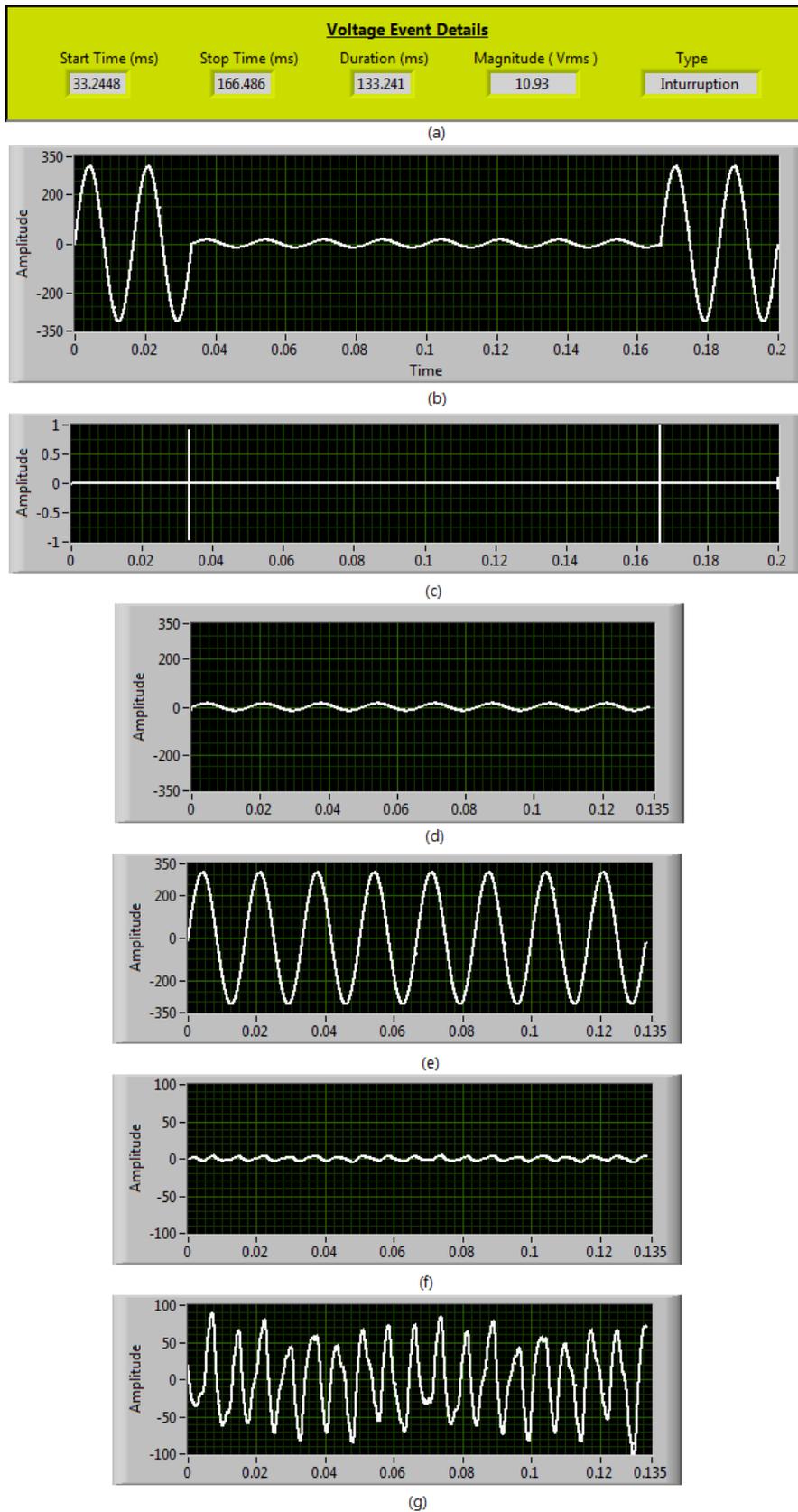
Fig. 15. Detection and classification of voltage interruption: a) details of the voltage interruption;
b) waveform of voltage interruption event; c) the 1st detail MRA level for (b); d) waveform of voltage
interruption during the disturbance time; e) waveform of nominal voltage during the disturbance time;
f) the coarsest approximation MRA level for (d); g) the coarsest approximation MRA level for (e).
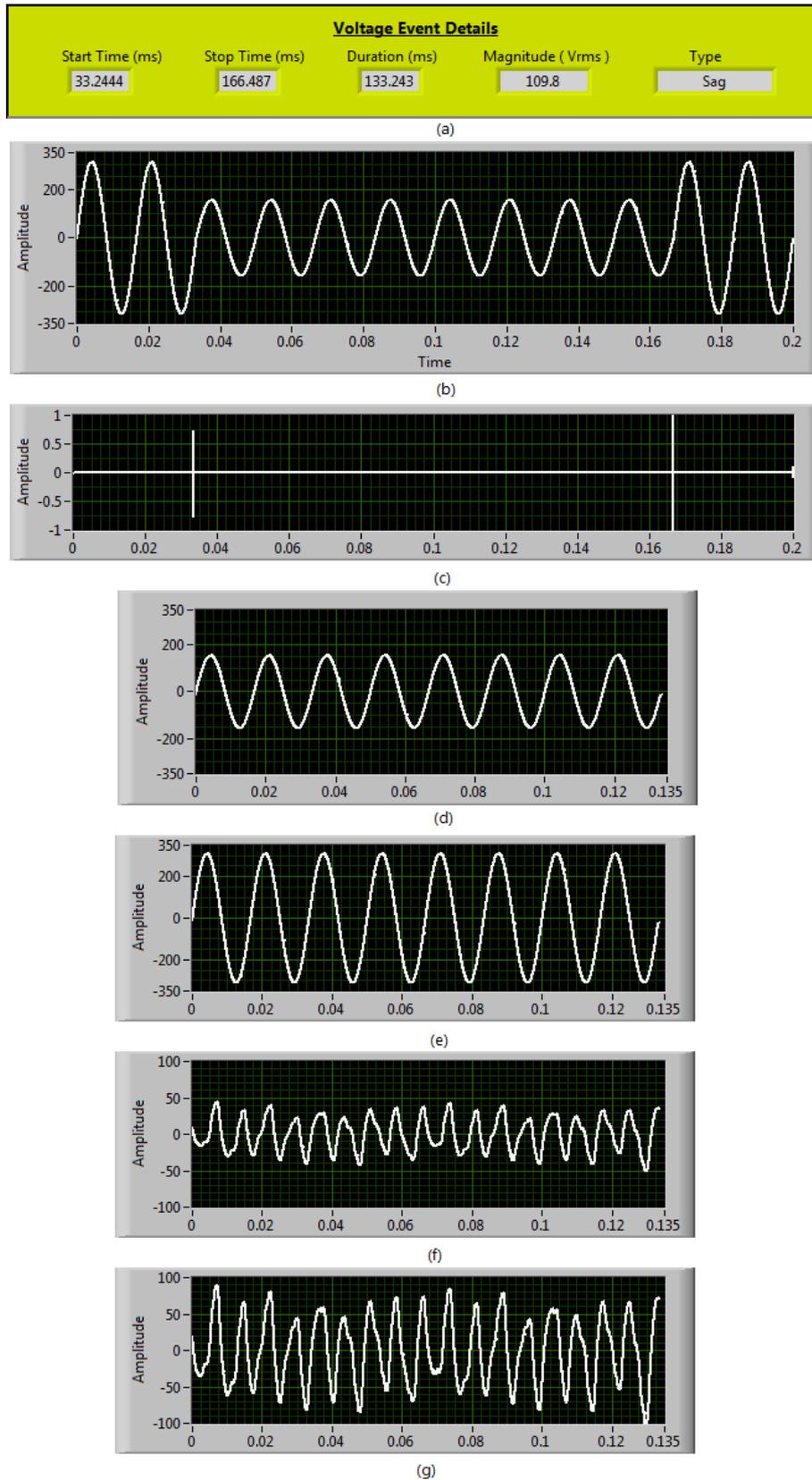
Fig.16. Detection and classification of voltage sag: a) details of the voltage sag; b) waveform of voltage sag event; c) The 1st detail MRA level for (b); d) waveform of voltage sag during the disturbance time; e) waveform of nominal voltage during the disturbance time; f) the coarsest approximation MRA level for (d); g) the coarsest approximation MRA level for (e).
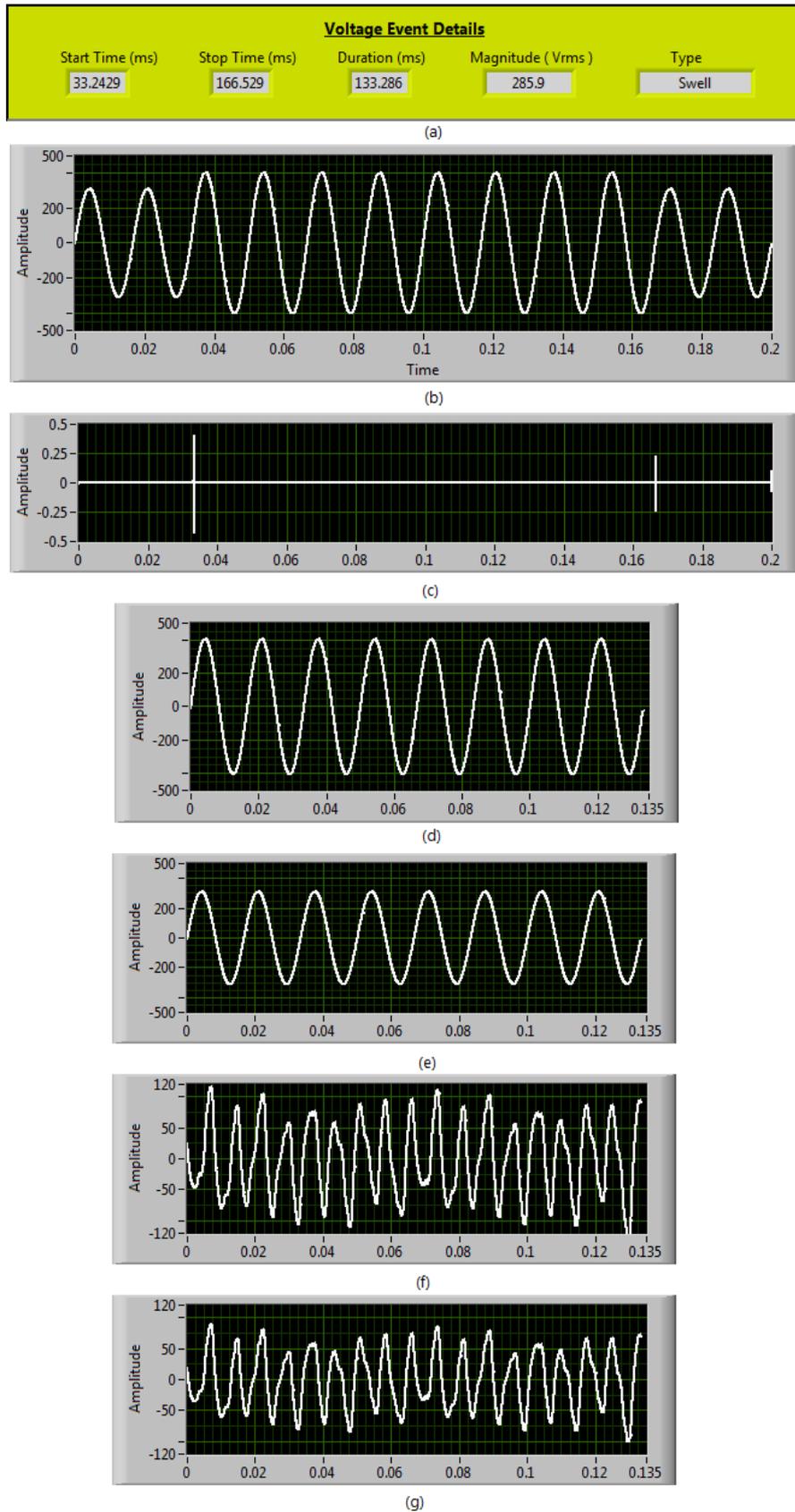
Fig. 17. Detection and classification of voltage swell: a) details of the voltage swell; b) waveform of voltage swell event; c) the 1st detail MRA level for (b); d) waveform of voltage swell during the disturbance time; e) waveform of nominal voltage during the disturbance time; f) the coarsest approximation MRA level for (d); g) The coarsest approximation MRA level for (e).

The accuracy measures of the proposed method in the characterization of voltage events in terms of the start time, end time, and magnitude are given in Table 2. The performance of the proposed approach is compared with the conventional method given in Eq. (19). It is quite evident that the accuracy of the proposed method is generally better than that of conventional methods although it utilizes less information. On the other hand, the average execution time for ten runs of the conventional method for analyzing data of one window (12 cycles) is 51 ms while the average execution time for ten runs of the proposed method for analyzing the same data size is 11 ms. The proposed method will save more than 78% from the processing time to accomplish the analysis of voltage events. This makes the proposed method more suitable for online implementation, simpler, and faster than the conventional one for calculating rms value.

Table 2. The proposed method accuracy for voltage events characterization.

Event characterization	Voltage event					
	Interruption		Sag		Swell	
	Conv.	Prop.	Conv.	Prop.	Conv.	Prop.
The start time	99.8	99.8	99.8	99.8	99.8	99.8
The stop time	99.7	99.7	99.7	99.7	99.6	99.6
The magnitude	98.7	99.2	99.9	99.8	98.8	99.9

6.4. Case 4- Voltage Events in the Presence of Harmonics

Fig. 18 shows the results of the proposed method for the start and end time detection of voltage events in the presence of harmonics. Fig. 18(a), (c) and (e) show the measured waveform corresponding to the monitoring system behavior in response to voltage sag, interruption and swell events in the presence of harmonics, respectively. The test case consists of voltage events in the presence of 3rd, 5th and 7th harmonics with 25, 15 and 10% harmonic contents, respectively. The start time, stop time and duration are 33.24 ms, 166.53 ms, and 133.29 ms for each voltage event. Fig. 18(b), (d) and (f) show the waveforms that are used to characterize and classify the voltage sag, interruption and swell. The estimated start time, end time and event duration are similar to those in Table 2.

As a conclusion from this experiment; the presence of harmonics does not affect the performance of the proposed method to detect, classify and characterize voltage events.
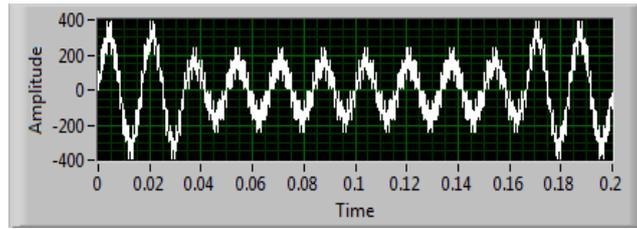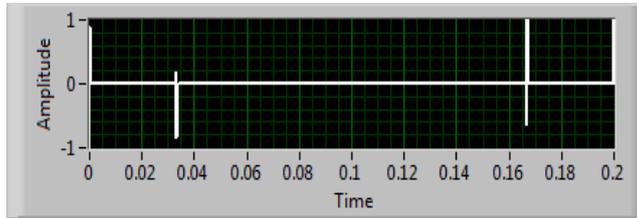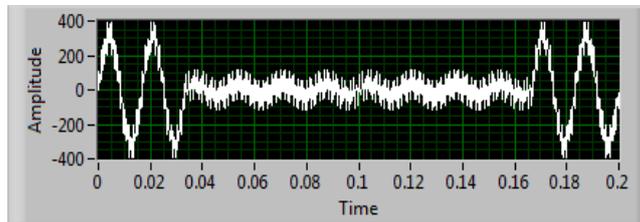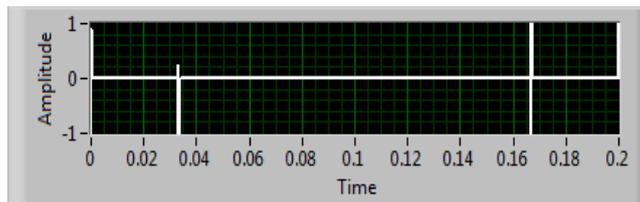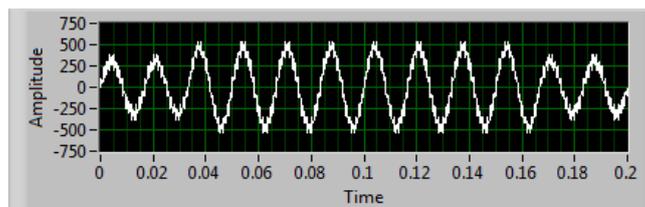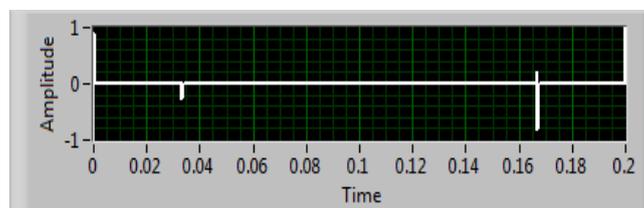
Fig. 18. Experimental results for detecting and classifying voltage events in the presence of harmonics:
a) voltage sag waveform in the presence of harmonics; b) the first detail MRA level for start and end time detection for (a); c) voltage interruption waveform in the presence of harmonics; d) the first detail MRA level for start and end time detection for (c); e) voltage swell waveform in the presence of harmonics; f) the first detail MRA level for start and end time detection for (e).

7. CONCLUSION

A new real-time voltage events detection and classification technique based on multi-resolution analysis has been proposed. The proposed technique utilizes the first detail level and the last approximation level to detect and classify voltage events. The laboratory setup of the proposed technique has been developed and built using LabVIEW platform. The experimental real-time results show effectiveness and robustness of the proposed technique in the detection of the start time, end time, and duration as well as the classification of all the voltage events considered. Moreover, the proposed method is less complex and faster than conventional methods.

REFERENCES

[1]   R. Dugan, M. Megranghan, H. Benty, *Electrical Power System Quality*, McGraw-Hill, New York, 2004.

[2]   EM Committee, "IEEE recommended practice for monitoring electric power quality," *IEEE Standard 1159*, 2009.

[3]   IEC, "Testing and measurement techniques- power quality measurement method," *IEC Standard 61000-4-30*, 2003.

[4]   A. de Almeida, L. Moreira, J. Delgado, "Power quality problems and new solutions," *International Conference on Renewable Power and Power Quality '03*, pp. 150-158, 2003.

[5]   S. Santoso, W. Grady, E. Powers, "Characterization of distribution power quality events with fourier and wavelet transforms," *IEEE Transactions on Power Delivery*, vol. 15, no. 1, pp. 247-254, 2000.

[6]   O. Poisson, P. Rioual, M. Meunier, "Detection and measurement of power quality disturbances using wavelet transform," *IEEE Transactions on Power Delivery*, vol. 15, no. 3, pp. 1039-1044, 2000.

[7]   S. Chen, H. Zhu, "Wavelet transform for processing power quality disturbances," *EURASIP Journal on Advances in Signal Processing*, vol. 2007, no. 1, pp. 1-20, 2007.

[8]   A. Shaik, A. Reddy, "Combined classification of power quality disturbances and power system faults," *2016 International Conference on Electrical, Electronics, and Optimization Techniques*, pp. 3796–3799, 2016.

[9]   M. Tuljapurkar, A. Dharme, "Wavelet based signal processing technique for classification of power quality disturbances," *2014 Fifth International Conference on Signal and Image Processing*, pp. 337–342, 2014.

[10] S. Khokhar, A. Zin, A. Mokhtar, M. Bhayo, A. Naderipour, "Automatic classification of single and hybrid power quality disturbances using wavelet transform and modular probabilistic neural network," *2015 IEEE Conference on Energy Conversion*, pp. 457–462, 2015.

[11] M. Valtierra-Rodriguez, R. Romero-Troncoso, R. Osornio-Rios, A. Garcia-Perez, "Detection and classification of single and combined power quality disturbances using neural networks," *IEEE Transactions on Industrial Electronics*, vol. 61, no. 5, pp. 2473-2482, 2014.

[12] R. GARG, B. Singh, D. Shahani, A. Chandra, K. Al Haddad, "Recognition of power quality disturbances using S-transform based ANN classifier and rule based decision tree," *IEEE Transactions on Industry Applications*, vol. 51, no. 2, pp. 1249-1258, 2014.

[13] M. Uyar, S. Yildirim, M. Gencoglu, "An effective wavelet-based feature extraction method for classification of power quality disturbance signals," *Electric Power Systems Research*, vol. 78, no. 10, pp. 1747-1755, 2008.

[14] M. Tuljapurkar, A. Dharme, "Wavelet based signal processing technique for classification of power quality disturbances," *2014 Fifth International Conference on Signal and Image Processing*, pp. 337-342, 2014.

[15] C. Naik, A. Chirag, P. Kundu, "Power quality index based on discrete wavelet transform," *International Journal of Electrical Power and Energy Systems*, vol. 53, pp. 994-1002, 2013.

[16] H. Jain, S. Gawre, "Detection and classification of current interruptions and transients by using wavelet transform and neural network," *2016 International Conference on Electrical Power and Energy Systems*, pp. 462–468, 2016.

[17] M. Gaouda, M. Salam, M. Sultan, A. Chikhani, "Power quality detection and classification using wavelet-multiresolution signal decomposition," *IEEE Transactions on Power Delivery*, vol. 14, no. 10, pp.1469–1476, 1999.

[18] W. Kanitpanyacharoean, S. Premrudeepreechacharn, "Power quality problem classification using wavelet transformation and artificial neural networks," *IEEE PES Power Systems Conference and Exposition*, vol. 3, pp. 1496-150, 2004.

[19] T. Zhu, S. Tso, K. Lo, "Wavelet-based fuzzy reasoning approach to power-quality disturbance recognition," *IEEE Transactions on Power Delivery*, vol. 19, no. 4, pp. 1928-1935, 2004.

[20] H. He, J. Starzyk, "A self-organizing learning array system for power quality classification based on wavelet transform," *IEEE Transactions on Power Delivery*, vol. 21, no. 1, pp. 286–295, 2006.

[21] T. Abdel-Galil, M. Kamel, A. Youssef, E. El-Saadany, M. Salama, "Power quality disturbance classification using the inductive inference approach," *IEEE Transactions on Power Delivery*, vol. 19, no. 4, pp. 1812-1818, 2004.

[22] M. Masoum, S. Jamali, N. Ghaffarzadeh, "Detection and classification of power quality disturbances using discrete wavelet transform and wavelet networks," *IET Science, Measurement and Technology*, vol. 4, no. 4, pp. 193-205, 2010.

[23] S. Mallat, "A theory for multiresolution signal decomposition: the wavelet representation," *IEEE Transactions on Pattern Analysis and Machine Intelligence*, vol. 11, no. 7, pp. 674–693, 1989.

[24] S. Mallat, *A Wavelet Tour of Signal Processing*, Academic Press, San Diego, 1999.

[25] H. Eristi, O. Yildirim, B. Eristi, Y. Demir, "Optimal feature selection for classification of the power quality events using wavelet transform and least squares support vector machines," *International Journal of Electrical Power and Energy Systems*, vol. 49, pp. 95-103, 2013.

[26] A. Rodriguez, J. Aguado, F. Martin, J. Munoz, M. Medina, G. Ciumbulea, "Classification of power quality disturbances using wavelet and artificial neural network," *International Conference on Power Systems and Technology*, pp. 1-7, 2010.

[27] H. Eristi, Y. Demir, "Automatic classification of power quality events and disturbances using wavelet transform and support vector machines," *IET Generation, Transmission and Distribution*, vol. 6, no. 10, pp. 968-976, 2012.

[28] F. Zaro, S. Ameenuddin, M. Abido, I. Elamin, "Characterization of short-duration voltage variations," *Proceedings of The 2012 IEEE International Power and Energy Conference*, pp. 650-654, 2012.

[29] M. Albu, G. Heydt, "On the use of rms values in power quality assessment," *IEEE Transactions on Power Delivery*, vol. 18, no. 4, pp. 1586-1587, 2003.

[30] N. Kagan, E. Ferrari, "Influence of rms variation measurement protocols on electrical system performance indices for voltage sags and swells," *9th IEEE International Conference on Harmonics and Quality of Power*, vol. 3, pp. 790–795, 2000.

[31] A. Moreno-Munoz, *Power Quality Mitigation Technologies in a Distributed Environment*, Springer, 2007.

[32] A. Parsons, W. Grady, E. Powers, "A wavelet-based procedure for automatically determining the beginning and end of transmission system voltage sags," *IEEE Power Engineering Society, 1999 Winter Meeting*, vol. 2, pp.1310–1315, 1999.

[33] V. Thiyagarajan, N. Subramaniam, "Wavelet approach and support vector networks based power quality events recognition and categorization," *2016 International Conference on Signal Processing, Communication, Power and Embedded System*, pp. 1667–1671, 2016.

[34] G. Swain, P. Sinha, M. Maharana, "Detection of islanding and power quality disturbance in micro grid connected distributed generation," *2017 International Conference on Innovative Mechanisms for Industry Applications*, pp. 388-393, 2017.